Validation and assessment of satellite-based columnar CO_2 and CH_4 mixing-ratios from GOSAT and OCO-2 satellites over India

Harish Gadhavi[1], Akanksha Arora[1,2], Chaithanya Jain[3], Mahesh Kumar Sha[4†], Frank Hase[5], Matthias Frey[6†], Srikanthan Ramachandran[1], Achuthan Jayaraman[3]

[1]Space and Atmospheric Science Division, Physical Research Laboratory, Ahmedabad, India
[2]Indian Institute of Technology Gandhinagar, Gandhinagar, India
[3]National Atmospheric Research Laboratory, Gadanki, India
[4]Royal Belgian Institute for Space Aeronomy, Brussels, Belgium
[5]Institute of Meteorology and Climate Research, Karlsruhe Institute of Technology, Karlsruhe, Germany
[6]National Institute for Environmental Studies, Tsukuba, Japan

[†]Formerly at Institute of Meteorology and Climate Research, Karlsruhe Institute of Technology, Karlsruhe, Germany

Correspondence to: Harish Gadhavi (hgadhavi@prl.res.in)

Abstract. Satellite observations of column-averaged carbon dioxide (XCO_2) and methane (XCH_4) mixing-ratios provide essential data for monitoring greenhouse gas emissions. However, the accuracy of emission estimates depends on the precision and bias of satellite retrievals, which require validation against ground-based reference measurements. This study presents a systematic validation of XCO_2 and XCH_4 data from GOSAT and OCO-2 satellites over South India using ground-based Fourier Transform Spectrometer (FTS) observations at Gadanki (13.5°N, 79.2°E) collected during October 2015 to July 2016. Satellite products from National Institute for Environmental Studies, Japan (NIES), NASA's Atmospheric CO_2 Observations from Space (ACOS) project, USA (ACOS), and the University of Leicester, UK (UoL) were evaluated using a three-step spatial-temporal pairing method. Results show that the UoL's proxy XCH_4 product meets the European Space Agency's Climate Change Initiative (ESA CCI) bias requirement (<10 ppb) across all spatial windows, while the NIES XCH_4 product meets the requirement only for intermediate spatial scales. For XCO_2, NASA ACOS and OCO-2 products meet the CCI bias requirement (<0.5 ppm), while NIES XCO_2 exceeds this threshold. All products satisfy the precision requirement (<8 ppm) with substantial margins. Additionally, FLEXPART model simulations using regional emission inventories revealed that agricultural activities dominate seasonal methane enhancements, contributing about 55%, followed by waste and wetland emissions. The model captured seasonal trends but underestimated the amplitude of observed variations, highlighting the influence of changing background methane levels. These findings demonstrate the suitability of recent satellite products for regional greenhouse gas monitoring and emphasize the need for expanding ground-based FTS networks across South Asia to support improved emission assessments.

1 Introduction

Carbon dioxide (CO_2) and methane (CH_4) are the two top most important greenhouse gases (GHGs) responsible for anthropogenic global warming. While the role of CH_4 in global warming is of primary interest, CH_4 also plays an important role in atmospheric chemistry by affecting OH amount, ozone production in remote areas and water (production) in the stratosphere (Fiore et al., 2002; Fleming et al., 2015; Laughner et al., 2021; Noel et al., 2018). Both CO_2 and CH_4 abundances in the atmosphere are on continuous rise post-industrial era (Dunn et al., 2022; Turner et al., 2022) and hence a continuous global monitoring of carbon dioxide and methane is highly desirable for identifying sources, sinks, trends and effective implementation of global treaties on reduction of greenhouse gases by individual countries. Satellites due

to their continuously improving data products, have come to be recognized as important tool in recent decade for monitoring and studying greenhouse gases. Satellites such as GOSAT (Greenhouse gases Observing SATellite) and OCO-2 (Orbiting Carbon Observatory-2) capture scattered solar radiation in the near infrared spectral region and provide columnar mixing ratios. GOSAT and OCO-2 are providing global coverage every 3 days and 16 days respectively (Table 1).

Table 1. Launch date, equator crossing time, revisit time for global coverage and sensor technology of satellites, the data of which are used in the study.

Name of satellite/sensor	Agency responsible for launch / maintenance	Launch Date	Equator crossing time	Satellite revisit time on same location	Greenhouse Gas related Data products	Principle of measurement
GOSAT aka Ibuki	JAXA, Japan / NIES, Japan	23 January 2009	13:00	3 days	Columnar CO_2 Columnar CH_4 CO_2 profile CH_4 profile	Fourier Transform Spectrometer
OCO-2 (Orbiting Carbon Observatory - 2)	JPL, USA	July 2014	13:35	16 days	Columnar CO_2	Diffraction grating Spectrometer

Satellite based estimates of greenhouse and trace gases have proved effective for deriving the emission fluxes (Bergamaschi et al., 2007, 2009; Bousquet et al., 2010; Chevallier et al., 2005). However, the improvement that can be achieved in emission fluxes depends highly on the accuracy of satellite retrievals. Climate Change Initiative (CCI) programme of European Space Agency (ESA) has listed the threshold precision and systematic error requirements for satellite derived columnar CO_2 and CH_4 mixing ratios (henceforth, columnar mixing ratios of CO_2 and CH_4 are represented by symbols XCO_2 and XCH_4 respectively), which are < 8 ppm precision and < 0.5 ppm systematic error for XCO_2 individual measurements, and < 34 ppb precision and < 10 ppb systematic error for XCH_4 individual measurements for deriving the regional emission fluxes of these species (Chevallier et al., 2016). WMO's Global Climate Observing System (GCOS) implementation plan has listed 1-sigma accuracy requirement of < 0.5 ppm for XCO_2 and < 5 ppb for XCH_4, respectively (GCOS-200, 2016).

To validate satellite-based estimates, standards against which the satellite observations can be compared are needed. The Total Carbon Column Observing Network (TCCON) operates high-resolution ground-based Fourier transform infrared spectrometers (FTS) for providing column-averaged greenhouse gas abundances with high accuracy and precision. TCCON observations serve as the reference data source for satellite validation. Recently, TCCON is supplemented by portable FTS operated in the framework of the Collaborative Carbon Column Observing Network (COCCON). TCCON currently operates more than 20 stations worldwide for high precision measurements of column average dry air mole fractions of CO_2, CH_4, N_2O, HF, CO, H_2O and HDO (https://tccon-wiki.caltech.edu; accessed in Sep 2024). All the sites follow common set of standards for instrumentation, data acquisition, calibration and analysis as prescribed by the TCCON Steering committee. TCCON sites use IFS 125HR FTS manufactured by Bruker Optics which cover a spectral range from 3900 cm^{-1} to 15500 cm^{-1} with a spectral resolution of 0.02 cm^{-1}. The calibration of TCCON is achieved using aircraft profiling over the sites. Errors in XCO_2 and XCH_4 are less than 0.16% and 0.4% respectively for solar zenith angle less than 82° (Laughner et al., 2024). While the XCO_2 and XCH_4 measured at TCCON sites are highly accurate and very important for validation of satellite, model and other instruments, the spectrometer is expensive, large and requires

continuous maintenance. The IFS 125HR FTS dimensions are of the order of 1 m x 1 m x 3 m and weighs several 100 kg, restricting its wide spread use or its deployment for short field campaigns or at remote sites with limited manpower. To supplement TCCON observations and to provide wider coverage of GHG observations, the Karlsruhe Institute of Technology (KIT) in collaboration with Bruker Optics, started developing a new type of portable FTS in 2011 which provides accurate measurement of GHGs while being lightweight and cost-effective. The prototype performance is described in Gisi et al. (2012). The spectrometer has become commercially available since 2014 under model designation EM27/SUN. Sha et al. (2020) compared the four different types of low-resolution spectrometers against IFS 125HR as well as in-situ observations using AirCore from one of the TCCON site over a period of 8 months and found EM27/SUN had the best performance matrix against high resolution spectrometer. COCCON is an emerging network of the portable FTS which uses tested and calibrated EM27/SUN spectrometers as well as common algorithms for data processing (Alberti et al., 2022a; Frey et al., 2019; Sha et al., 2020). Support for calibration and data processing is provided by KIT and the COCCON spectrometers are calibrated against TCCON by performing side-by-side observations. Today, more than 83 EM27/SUN spectrometers are operated worldwide under COCCON network (Alberti et al., 2022a). The portability of EM27/SUN spectrometer and high accuracy in retrieving XCO_2 and XCH_4 have made the instrument and COCCON network being used in a variety of applications. Pak et al. (2023) and Herkommer et al. (2024) have used EM27/SUN spectrometer as travelling standard to evaluate consistency of TCCON measurements. Frausto-Vicencio et al. (2023) have used EM27/SUN spectrometer to estimate combustion efficiency of wild fires at regional scale. Stremme et al. (2023) have used the spectrometer to study CO_2 plumes from volcano. Dietrich et al. (2021) and Alberti et al. (2022b) have used them for detecting city scale gradient in the gas mixing ratios and identifying the sources of emissions.

An assessment conducted by Buchwitz et al. (2017) using TCCON sites found that GOSAT and OCO-2 meet the requirements set by ESA's CCI Programme and WMO's GCOS implementation plan across various parts of the world. However, due to a lack of data, this systematic assessment has so far not been conducted over South Asia. However, there have been studies that compared satellite data with ground-based FTS observations from Shadnagar (17°05′ N, 78°13′ E), near Hyderabad, Telangana—a city in the south-central part of India. Sagar et al. (2022) compared XCH_4 values from Sentinel-5P/TROPOMI (from December 2021 to March 2021) with ground-based FTS observations and found a mean bias of 3.61 ppb. Pathakoti et al. (2024) compared XCO_2 data from the OCO-2 satellite with ground-based FTS and reported a mean bias of 3.81 ppm and a root mean square error (RMSE) of 6.6 ppm. Pathakoti et al. (2024) used version 8 bias-corrected OCO-2 data. Aside from these few studies, no systematic ground validation of satellite data for GHGs has been conducted over the South Asian region. Additionally, there has been no validation of GOSAT over South Asia. Since the release of version 8 of OCO-2 data, several improvements have been made to the OCO-2 algorithm, and the latest version (v11.1) is now available to public users (Jacobs et al., 2024).

National Atmospheric Research Laboratory (NARL), Gadanki and Institute for Meteorology and Climate Research (IMK-ASF) of Karlsruhe Institute of Technology (KIT), Karlsruhe collaborated to make XCO_2 and XCH_4 measurements over South India using a portable Fourier Transform Spectrometer (FTS) similar to the one in COCCON network. In this manuscript, we present a systematic validation of XCO_2 and XCH_4 estimated from GOSAT and OCO-2 over a site in South Asia using ground-based measurements and using the latest retrieval algorithms.

2 Instrumentation and Data

In this study, a commercial low resolution (0.5 cm^{-1}) FTS (Model: EM27/SUN FTS Make Bruker) with modified sun-tracker and InGaAs detector is used. The spectrometer has high thermal and mechanical stability and 0.5 cm^{-1} spectral resolution in the spectral range 5000 to 9000 cm^{-1}. Sun-tracker system developed at KIT uses live sun image to guide sun-

tracker for accurate position of sun-beam on the field stop. This allows far more precise sun-tracking even when intensity over the sun disk is varying due to cloud or other factors. The tracking accuracy achieved is of the order of 11 arc sec (Gisi et al., 2011). A detailed description of the instrument can be found in Gisi et al. (2012). The instrument used has been calibrated by performing side-by-side measurements next to the TCCON spectrometer in Karlsruhe. The instrument is calibrated for specific deviations from nominal instrumental line shape (ILS) and the absence of any other systematic errors is verified at KIT. Details about the ILS measurement and data analysis as well as the comparison of calibration factors between the COCCON spectrometers have been discussed in Frey et al. (2019), Sha et al. (2020) and Alberti et al., (2022a). Sha et al. (2020) have found a mean bias of -0.18±0.45 ppm and 0.003±0.005 ppm between EM27/SUN and TCCON instrument for XCO_2 and XCH_4 respectively. The XCO_2 and XCH_4 scaling factors derived from side-by-side measurements between the spectrometer used in this study (Instrument Serial No. 52) and the COCCON reference spectrometer (Instrument Sr. No. 37) were determined to be 0.999482 and 1.000825, respectively, prior to the start of observations at Gadanki (Alberti et al., 2022a). In addition to solar spectra, measurements of atmospheric parameters like temperature and pressure were also obtained near the spectrometer.

2.1 Ground-based FTS

The recorded spectra are analysed using retrieval code PROFFAST v2.4 developed at KIT (KIT IMK-ASF 2024a). PROFFAST software retrieves the gas amount by fitting solar absorption spectra and scaling the a priori atmospheric profiles of the gases. It was run using a python interface PROFFASTpylot v1.3 which also takes care of preprocessing of raw instrument data (Feld et al., 2024; KIT IMK-ASF 2024b). The PROFFAST algorithm is validated in several studies and used across all the COCCON sites to provide uniform and consistent data processing (Frey et al., 2019; Gisi et al., 2012; Hase et al., 2004; Sepúlveda et al., 2012; Sha et al., 2020). The spectral windows used for different species are shown in Table **2**. The algorithm requires vertical profiles of temperature and pressure and a priori estimates of profiles of species to be estimated. Vertical profiles of temperature and pressure are obtained from National Center for Environmental Prediction (NCEP) reanalysis data corresponding to the dates of observations. The a priori estimates of species profiles are obtained from WACCM (Whole Atmosphere Community Climate Model) (Marsh et al., 2013) which is the average of 40 year monthly mean values for the site. The preprocessing step involves quality check of interferogram, DC correction, fast fourier transform, phase correction and resampling of the spectra. Each record of raw data is a set of 10 spectra of which 5 are captured when the mirror is moving forward and 5 are captured when the mirror is moving backward. The interferogram is checked for signal level and source brightness fluctuations also known as DC variability and is removed from further analysis if threshold levels are not met. The other measurement and instrument specific corrections included in the processing are DC correction (correction for the sun brightness fluctuations) (Keppel-Aleks et al., 2007) and the application of instrumental line shape (ILS) parameters (Abrams et al., 1994; Alberti et al., 2022a; Hase et al., 1999; Messerschmidt et al., 2010). As the first step, the columnar concentrations of CO_2, CH_4, O_2 and H_2O in terms of number of molecules per m^2 are retrieved. Then, the CO_2 and CH_4 concentrations are converted to column average mixing ratios by assuming O_2 mixing ratio as 20.95% and normalising CO_2 and CH_4 concentrations with respect to O_2. This allows for compensating various systematic errors. XCO_2 measurement precision is 0.13 ppmv and XCH_4 measurement precision is 0.6 ppbv (Frey et al., 2019).

Table 2. **List of spectral windows used for retrieving columnar concentrations of various gases using ground-based FTS**

Species	Spectral windows used for analysis
CH_4	5897 – 6145 cm^{-1}
CO_2	6173 – 6390 cm^{-1}

O_2	7765 – 8005 cm^{-1}
H_2O	8353.4 – 8463.1 cm^{-1}

Observations were carried out from October 2015 to July 2016 in the Gadanki campus of NARL. Gadanki (Latitude: 13.45° N, Longitude: 79.18° E, 360 m above mean sea level) is a rural site in South India with a tropical wet climate. It experiences two monsoon seasons known as southwest and northeast monsoon seasons. Change in wind circulation from one season to the other season is known to have significant effect on trace-gases and aerosol concentrations at the site (Renuka et al., 2014; 2020; Suman et al., 2014). The site is surrounded by hilly terrain and the nearest city is about 35 km away. A major part of the terrain surrounding Gadanki is forest and farm lands. Though there is no farming of rice (paddy field) in the immediate vicinity, the region as a whole has a good number of paddy fields. More details about the site and various atmospheric observation facility can be found in Pandit et al. (2015) and Jayaraman et al. (2010). The FTS observations were carried out from morning to evening at an interval of 1 minute except during days with inclement weather and weekends. More than 39,000 spectra covering a period of 10 months were analysed to retrieve XCO_2 and XCH_4.

2.2 GOSAT

The greenhouse gases observing satellite (GOSAT) also known as IBUKI is a joint project of the Ministry of the Environment (MoE), Japan, the National Institute for Environmental Studies (NIES), Japan and the Japan Aerospace Exploration Agency (JAXA), Japan (Yokota et al., 2009). The main instrument onboard GOSAT is a Thermal and Near infrared Sensor for carbon Observations (TANSO) (Table 1). It is a Fourier transform spectrometer (FTS) with two detectors, one for shortwave infrared (SWIR) wavelength range and the other for thermal infrared (TIR) wavelength range (Olsen et al., 2017). While the TIR sensor is used to retrieve CO_2 and CH_4 profiles, the SWIR sensor is used to retrieve column average dry mole fraction of CO_2 (XCO_2) and CH_4 (XCH_4). In the current study, only XCO_2 and XCH_4 values from SWIR sensor are used.

The column-averaged dry-air mole fractions of methane (XCH_4) and carbon dioxide (XCO_2) retrieved from GOSAT are available from three different sources: (1) National Institute for Environmental Studies (NIES), Japan, (2) UK National Centre for Earth Observation at University of Leicester (UoL), UK, and (3) the Goddard Earth Science Data Information and Services Center (GES DISC) of National Aeronautics and Space Administration (NASA, USA).

NIES Data Products:

NIES provides operational XCH_4 and XCO_2 products using a full physics algorithm, which minimizes the difference between observed and simulated spectra generated by a radiative transfer model (Someya et al., 2023). In the current study, we use bias-corrected FTS SWIR Level 2 v3.05 data products from NIES, hereafter referred to as NIES XCH_4 or NIES XCO_2.

UoL Data Products:

UoL provides XCH_4 data derived using a proxy retrieval approach (Parker et al., 2020). This method first retrieves the XCH_4/XCO_2 ratio from the common absorption band near 1.6 μm, and then estimates XCH_4 by multiplying this ratio with a model-derived XCO_2 value. The advantage of this approach is its reduced sensitivity to aerosols, thin cirrus clouds and certain instrumental effects. However, reliance on model-based XCO_2 can introduce biases in the retrieved XCH_4. To mitigate this, UoL uses the median of XCO_2 estimates from three different atmospheric models constrained by surface in-situ observations. In the current study, we use UoL Version 9 XCH_4 data, hereafter referred to as UoL XCH_4.

NASA ACOS Data Products:

NASA's GES DISC provides XCO_2 products retrieved under the Atmospheric CO_2 Observations from Space (ACOS) project (Osterman et al., 2017), using a full physics algorithm originally developed for the OCO satellite and later adapted

for GOSAT. In the current study, we use ACOS Level 2 bias-corrected XCO_2 Version 9.2 data, hereafter referred to as ACOS XCO_2.

2.3 OCO-2

Orbiting Carbon Observatory-2 (OCO-2) is NASA's Earth remote sensing satellite to study atmospheric carbon dioxide from space (Crisp et al., 2004). In the current work, we have used processed and bias corrected data version 11.1r downloaded from the website of GES DISC (http://disc.gsfc.nasa.gov/). Version 11.1r is the latest version of data which were released in May 2023. The version 11.1r data contains retrospectively retrieved XCO_2 values using full physics algorithm with several improvements with respect to its predecessor algorithms (Jacobs et al., 2024; Payne et al., 2023). The OCO-2 was launched on July 2, 2014 in sun-synchronous orbit with equatorial crossing time at 13:30 on an ascending node with 16 days repeat cycle (Table 1). OCO-2 instrument consists of three boresight high resolution imaging grating spectrometers which provides high resolution spectra of reflected sun light in oxygen A band (0.765 μm) and in two CO_2 bands at 1.61 and 2.06 μm. The instruments can be operated in three modes viz., target, glint and nadir. The ground resolution varies depending on the mode of operation. In the current study, data from the nadir mode are used which has the spatial resolution of 1.29 km x 2.25 km (Crisp et al., 2017). The spectra are corrected for various artefacts such as bad pixels, cosmic ray artefacts and converted to radiometric values. Using full physics radiative transfer model, synthetic spectra are produced and compared with observed spectra. An inverse model iteratively modifies the assumed atmospheric state to improve the fit. The number densities of CO_2 and O_2 thus retrieved are used to get XCO_2 by taking ratio of them and multiplying it by 0.2095. The retrieval is further applied bias correction obtained from collocated TCCON data, models and small area analysis (O'Dell et al., 2018). More details of the retrieval process are available in Crisp et al. (2021). The OCO-2 data are distributed in two formats known as standard files and Lite files. The standard files contain CO_2 mixing-ratios without bias correction whereas mixing-ratios in the Lite files are bias corrected (Payne et al., 2023). The data files contain a quality flag for each retrieval. The quality flag value "0" corresponds to good data, whereas the quality flag value "1" suggests the presence of any of the 24 algorithmically identified quality issues in the retrieved value. In the present work, we have used bias corrected data with quality flag "0" only.

3 FLEXPART (A Lagrangian Particle Dispersion Model)

Besides, comparing satellite data with ground-based observations, we have also examined the seasonal variation of methane mixing ratios using a Lagrangian Particle Dispersion Model to understand the influence of local sources vis-a-vis long-range transport. The FLEXPART (Pisso et al., 2019), an open source model developed at Norwegian Institute for Air Research (NILU), Kjeller, Norway is widely used by the research community around the world to identify the source regions of long range transport. The model takes meteorological fields as input and tracks the movement of virtual particle forward or backward in time. The particle can be configured to represent a gas or aerosols of one's choice and accordingly be subjected to various physical processes such as advection, turbulence, dry deposition, wet deposition, radioactive decay, etc. Except for reaction with OH radical no other chemical transformation is modelled in FLEXPART.

We configured FLEXPART for backward-in-time run from observation site (Gadanki) with virtual particle representing methane molecules. The backward-in-time runs provide a source-receptor relationship which can be used to calculate mixing ratios or concentrations at observation site using emission fluxes. The model run is configured such that mixing ratios thus calculated represent results of emissions within the past 10 days and average of 0 to 15 km atmospheric column at the observation site. This configuration effectively captures most regional emissions and tropospheric methane mixing

ratios. Using few sensitivity tests, we have found that emissions within 10 to 15 days have insignificant contribution to concentrations beyond 15 km. More details of the model settings used for the current study are provided in Table 3.

Table 3. The FLEXPART model setup and the input data details

Input Meteorological Data	ECMWF Reanalysis – Interim (ERA-Interim) (Dee et al., 2011)
Tracer	CH_4
Point of origins for retroplume (aka Release Point)	Gadanki Latitude: 13.45° N Longitude: 79.18° E, Site altitude: 365 m a. s. l. Plume release altitudes from ground: 0 – 15 km.
Number of particles released for each day	100000
Mode	Backward runs
Number of days backward for each release	10 days
User selectable Processes	Dry Deposition – disabled Convection – enabled Wet deposition – disabled Reaction with OH radical – enabled
OH reaction related settings	Constants $C = 9.65 \times 10^{-20}$ cm^3 $molecule^{-1}$ sec^{-1} D = 1082.0 K N = 2.58 (no unit)

3.1 ECLIPSEv6 inventory

In order to calculate the concentrations resulting from recent regional emissions (emissions within past 10 days of a given observation), we used ECLIPSEv6b (**E**valuating the **CL**imate and air quality **I**m**P**acts of **S**hort-liv**E**d pollutants version 6b) emission inventory (Amann et al., 2011, 2012; Klimont et al., 2017; Hoglund-Isaksson, 2012; Stohl et al., 2015). The inventory is prepared following IPCC (2008) recommended method and using Greenhouse Gas - Air Pollution Interactions and Synergies (GAINS) model (Amann et al., 2011). It provides sector-specific anthropogenic emission estimates for 11 species, including CH_4, across eight economic sectors. The data are provided as 0.5° x 0.5° gridded values for the years from 1990 to 2050 at an interval of 5 years for two scenarios namely current legislation for air pollution, which is also the reference scenario and maximum technically feasible reductions scenario. The latest version (Version 6b) was released in August 2019 and incorporates updates for historical data, new waste sectors, soil NO_X emissions, international shipping emissions and energy-macroeconomic data. The inventory includes only anthropogenic emission fluxes from sectors viz. energy, industry, solvent use, transport, domestic combustion, agriculture, open biomass and agricultural waste burning, and waste treatment. Natural emissions from wetlands, forest fires, biogenic emissions, etc. are not included in the inventory. The total Global, South Asia (members of SAARC – South Asian Association for Regional Cooperation), and India's emissions of methane for the year 2015 were 336.2, 44.2 and 31.5 Tg, respectively.

3.2 Wetland Inventory

The emissions from wetlands can contribute significant atmospheric load of methane at the observation site and hence in addition to anthropogenic emissions from ECLIPSEv6 inventory, we used Wetland CH_4 emissions and uncertainty dataset

for atmospheric chemical transport models (WetCHARTs) version 1.0 inventory (Bloom et al., 2017a, b) for calculating methane concentrations at Gadanki from recent emissions. The inventory contains global monthly emission fluxes of methane at 0.5° by 0.5° resolution for ensemble of multiple terrestrial biosphere models, wetland extent scenarios and temperature dependencies. The emission fluxes from 2001-2015 are provided for three choices of global scaling, two choices of wetland spatial extent, two choices for temporal variability of wetland extent, nine choices of heterotrophic respiration schemes and three choices of parametrization scheme for temperature dependency. In the current work, we have used data corresponding to the scaling factor with global emissions 166 $TgCH_4\ yr^{-1}$, CARDAMOM (**CAR**bon **DA**ta **MO**del fra**M**ework) terrestrial C cycle analysis for heterotrophic respiration (Bloom et al., 2016), mid-range temperature sensitivity and, spatial and temporal extent of wetlands constrained with SWAMPS (**S**urface **WA**ter **M**icrowave **P**roduct **S**eries) multi-satellite surface water product (Schroeder et al., 2015). These choices are made based on following consideration. Choice of scaling factor represents the mid-point global emissions among the three choices available viz. 124.5, 166 and 207.5 Tg CH_4/yr. While there are nine choices for heterotrophic respiration, there is only one choice available for emission fluxes after 2010 which is CARDAMOM and used here. Between the two choices of spatial extent and two choices of temporal variability, the SWAMPS multi-satellite surface water product is used because it represents observationally constrained inundated areas including lakes and other water bodies.

4 Results and Discussion

Box plots of monthly statistics are shown in Figure 1 for (a) XCH_4 and (b) XCO_2 measured by EM27/SUN at the Gadanki site. Figure 2 shows the time series of hourly mean values of XCH_4 and XCO_2 from EM27/SUN, NIES, UoL, ACOS and OCO-2 within box size ±30° longitude and ±10° latitude of the site (Table 4). A large variability in XCH_4 values is observed in October, but in other months, the variability is relatively low. The median values of XCH_4 are found to systematically decrease from 1.892 ppm in October to 1.826 ppm in June of the following year, with similar values observed in July. The monthly median values of XCO_2 increased from 396.4 ppm in October to 405.8 ppm in May, then began to decrease after May. Unlike XCH_4, the XCO_2 values did not show high variability in October. A similar seasonal variation was observed by Jain et al., (2021) in surface mixing ratios of CO_2 and CH_4 at Gadanki. Kavitha and Nair (2016) using SCIAMACHY satellite data over India for the period 2003-2009, also reported similar seasonal variations, attributing them to regional rice cultivation patterns. Further discussion on the seasonal variation is provided in the subsequent section.

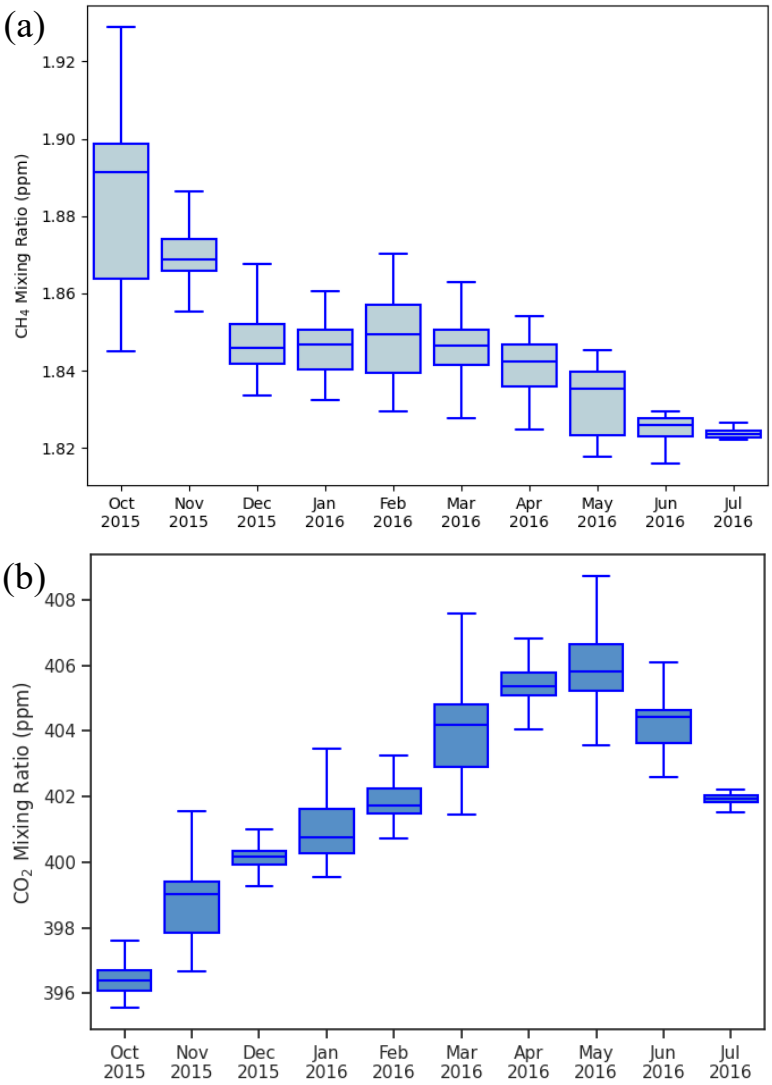

Figure 1. Box plot of monthly statistics of (a) CH_4 and (b) CO_2 columnar mixing ratios observed at Gadanki, India using ground-based FTIR.

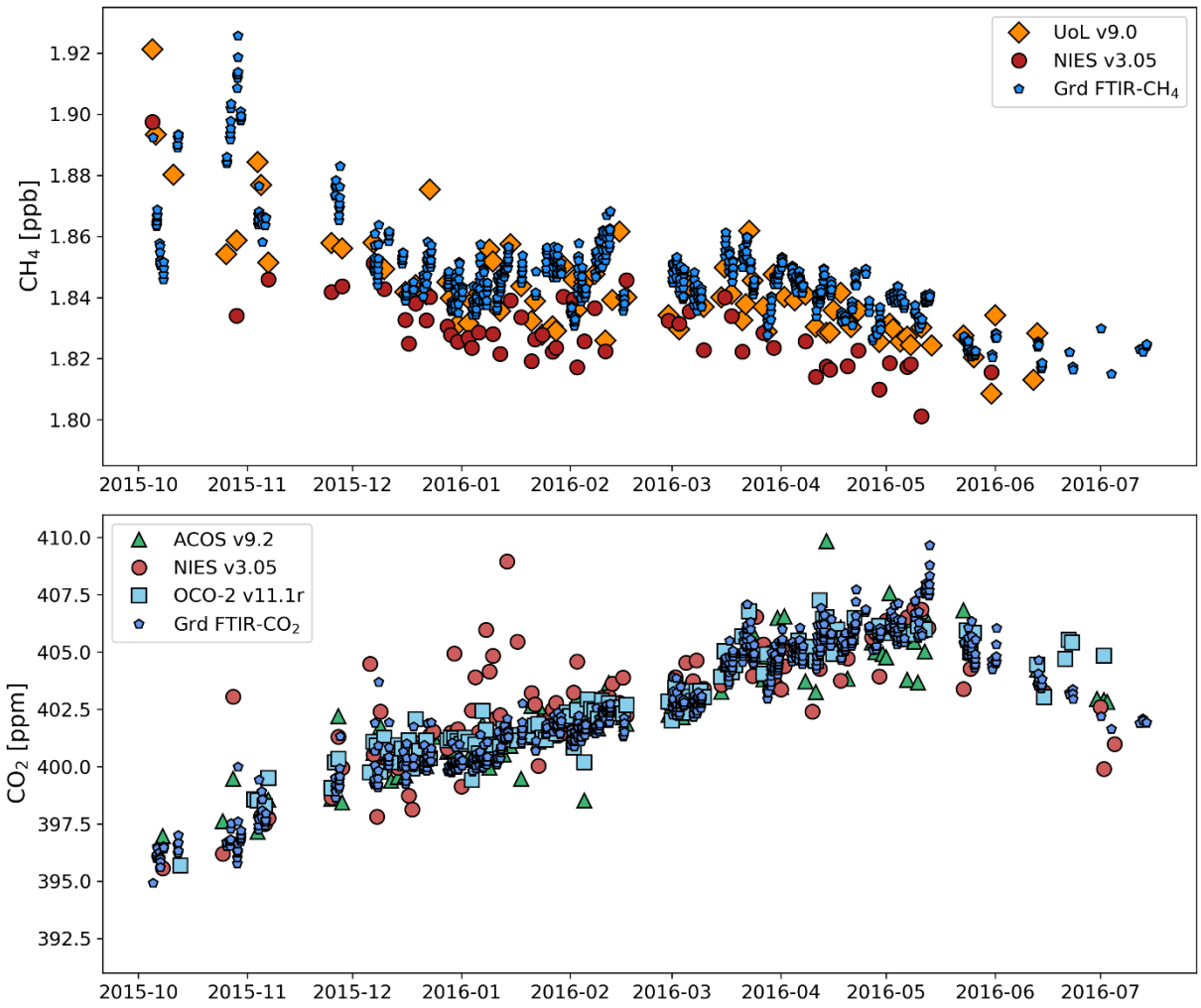

Figure 2. Hourly mean values of columnar CH_4 (top) and CO_2 (bottom) mixing ratios observed using ground based FTIR along with paired satellite observations. See the text for description of pairing method (Box size ±30° longitude and ±10° latitude)

4.1 Comparison of satellite-based and ground-based mixing-ratios

The GOSAT satellite revisits the same point on Earth every three days, with retrievals performed only under cloud-free sky conditions. This limits the number of concurrent satellite and ground-based FTIR measurements. To address this limitation and ensure sufficient data pairs for comparison, we have followed an approach similar to Buchwitz et al. (2017). This approach relies on the fact that CO_2 and CH_4 have long atmospheric residence times, allowing the history of air parcels to be used to pair data for comparison.

In this approach, the first step is to identify all satellite data within a certain distance of the ground station. Buchwitz et al. (2017) used satellite data within ±30° longitude and ±10° latitude of TCCON sites to evaluate GOSAT and OCO-2 data products. Wunch et al. (2017) used box of ±5° longitude and ±2.5° latitude around the TCCON sites in the Northern Hemisphere and ±60° longitude and ±10° latitude around the TCCON sites in the Southern Hemisphere to evaluate XCO_2 estimates from the OCO-2 satellite. In the second step, ground-based observations taken within three days of the satellite overpass and during same time of the day (within two hours) are paired with the satellite data. In the third step, the data pairs obtained in step 2 are further filtered using the criterion that the CAMS model output of XCH_4 and XCO_2 values, interpolated to the satellite location and ground station, cannot differ by more than 0.25 ppm for XCO_2 and 5 ppb for XCH_4, respectively. This third step is based on the premise that the CAMS model is capable of simulating transport accurately, meaning that while the absolute values may not always be correct, the spatial variability in the model is reliable. The criteria in step 3 ensures that satellite and ground values are only compared when they share the same air mass

history. It should be noted that the absolute value of the model simulation and its differences with observations are not relevant in this step. More detailed discussions on the need and the rationale behind this complex approach for data pairing can be found in Nguyen et al. (2014) and Wunch et al. (2011b). A sensitivity test, described in Table S1 of the Supplement, shows omitting the model-based air mass filtering (Step 3) increases the number of matched pairs by factors of 2 – 3 across species and datasets. While the effect on bias is mixed, the scatter generally increases slightly when Step 3 is not applied. For consistency with previous studies, we report results based on the full three-step pairing procedure.

We note that no averaging kernel (AK) correction were applied in this analysis. While applying AK corrections is ideal to account for vertical sensitivity differences between satellite and ground-based retrievals, effect of their omission is expected to be small for our study location. Sha et al. (2021) demonstrated that at low-latitude sites, the impact of smoothing and a priori profile differences on XCH_4 biases is minor, typically below -0.25%, with an average effect of -0.14%. Given that Gadanki (13.5° N) is a low-latitude station, the lack of AK correction is unlikely to significantly affect our conclusions.

We performed calculations for three different box sizes around the observation site at Gadanki (13.45° N, 79.18° E): (±5° longitude, ±2.5° latitude), (±10° longitude, ±5° latitude), and (±30° longitude, ±10° latitude). By the end of the third step, we obtained 55 pairs of XCH_4 from GOSAT NIES v3.05, 81 pairs of XCH_4 from GOSAT UoL v9, 117 pairs of XCO_2 from GOSAT v3.05, 117 pairs of XCO_2 from ACOS v9.2 and 120 pairs of XCO_2 from OCO-2 v11.1 for the biggest box-size in Step 1 (see Table 4, Figure 2). The number of data pairs for XCO_2 is more than double that of XCH_4 for all box-sizes. This difference reflects the fact that carbon dioxide has a much longer atmospheric lifetime (>100 years) compared to methane (~12 years).

Table 4: Mean bias and scatter between satellite and ground-based measurements. Values that meet CCI criteria are shown in bold letters.

Satellite	Species	Product version	Box Size for pairing		Number of data points	Bias = mean (Xsat - Xgrd)*	Scatter = stddev(Xsat - Xgrd)*	Pearson correlation coefficient R
			Longitude	Latitude				
GOSAT	XCH_4	NIES v3.05	±30	±10	55	-18.5 ppb	**13.8 ppb**	0.47
			±10	±5	19	**-9.07 ppb**	**12.1 ppb**	0.75
			±5	±2.5	12	-12.8 ppb	**6.21 ppb**	0.85
		UoL v9.0	±30	±10	81	**-5.6 ppb**	**15.0 ppb**	0.58
			±10	±5	39	**-0.6 ppb**	**13.6 ppb**	0.7
			±5	±2.5	24	**-2.0 ppb**	**7.9 ppb**	0.86
	XCO_2	NIES v3.05	±30	±10	117	0.644 ppm	**1.69 ppm**	0.74
			±10	±5	59	0.812 ppm	**1.88 ppm**	0.59
			±5	±2.5	27	0.983 ppm	**1.59 ppm**	0.67
		ACOS v9.2	±30	±10	117	**0.156 ppm**	**1.09 ppm**	0.90
			±10	±5	54	**0.077 ppm**	**1.25 ppm**	0.86
			±5	±2.5	24	**-0.212 ppm**	**1.02 ppm**	0.90
OCO-2	XCO_2	V11.1r	±30	±10	120	**0.408 ppm**	**0.776 ppm**	0.94
			±10	±5	67	**0.342 ppm**	**0.806 ppm**	0.94
			±5	±2.5	41	**0.163 ppm**	**0.786 ppm**	0.95

*Xsat are satellite based mixing ratio estimates and Xgrd are ground based FTIR mixing ratio

estimates. For all the satellites, their bias corrected values are used.

With the paired dataset in place, we evaluated the bias, scatter, and correlation between satellite and ground-based measurements, as summarized in Table 4. Here, bias is defined as the mean of difference between satellite- and the ground-based dry-air mole fractions, scatter as the standard deviation of these differences, and correlation as the Pearson correlation coefficient (R) between the paired values. The European Space Agency's Climate Change Initiative (ESA CCI) specifies performance targets of < 34 ppb for scatter (precision) and < 10 ppb for bias (systematic error) for XCH_4, and <8 ppm for scatter and <0.5 ppm for bias for XCO_2 (Chevallier et al., 2016).

XCH_4 Validation Results

For GOSAT NIES XCH_4, biases ranged from -9 ppb to -18.5 ppb depending on the spatial window size. For GOSAT UoL XCH_4, biases were notably lower, ranging from -0.6 ppb to -5.6 ppb. While larger spatial windows provided more matched pairs, they did not consistently yield lower bias or scatter. In fact, the intermediate box size (±10° x ±5°) showed the lowest bias and scatter for both products. Importantly, biases across all box sizes remained within one standard deviation of the smallest box size, indicating that larger spatial windows may not offer significant additional value, particularly when longer time series of ground-based data are available.

The UoL XCH_4 product met the ESA CCI bias requirement (< 10 ppb) across all box sizes. In contrast, the NIES XCH_4 products met this requirement only for the intermediate box, with marginal exceedances for the smallest box. Scatter values ranged from 6 ppb to 15 ppb across products and box sizes, well within the CCI precision requirement of 34 ppb. Although derived from the same satellite, the UoL XCH_4 product, which uses a proxy retrieval approach, showed substantially improved bias performance compared to the NIES product. However, its scatter was slightly higher (approx. 2 ppb) than the NIES product for equivalent spatial windows ranging from 8 to 15 ppb.

XCO_2 Validation Results

All XCO_2 products showed high correlation with ground-based measurements across all spatial windows. Biases for GOSAT NIES XCO_2 ranged from 0.644 ppm to 0.983 ppm, exceeding the CCI bias threshold of 0.5 ppm for all box sizes. However, scatter values (1.59–1.88 ppm) were well below the 8 ppm precision requirement.

In contrast, ACOS v9.2 XCO_2, also based on GOSAT observations but using a different retrieval algorithm, demonstrated superior performance. Biases ranged from -0.212 ppm to 0.163 ppm, meeting the CCI bias requirement across all box sizes. Scatter ranged from 1.02 ppm to 1.25 ppm, also comfortably within the precision target. Correlation coefficient (R = 0.86–0.90) for ACOS XCO_2 were higher than those for NIES XCO_2 (R = 0.59 – 0.74).

The OCO-2 XCO_2 v11.1r product showed the highest correlation among all datasets (R = 0.94 – 0.95), with biases ranging from 0.163 ppm to 0.408 ppm, fully meeting the CCI bias target. Scatter values (0.776 – 0.806 ppm) were the lowest among all products evaluated.

Our results for OCO-2 XCO_2 differ notably from the higher bias of 3.81 ppm reported by Pathakoti et al. (2024) for Shadnagar, India, located about 500 km north of our study site. While Pathakoti et al. have not discussed the reason for such a high bias in their study, it is unlikely to be solely due to the use of an earlier version of the OCO-2 dataset by them. Pairing methodology differences between our study and that of Pathakoti et al. may have contributed to the difference in results. Their study used a smaller spatial window (4° × 4°) and daily mean ground-based values, whereas we applied a larger spatial window (10° × 5°), used hourly collocation within ±2 hours, and applied model-based air mass filtering to improve representativeness. Additionally, Pathakoti et al. did not specify the retrieval algorithm version for their ground-based FTS data. Pak et al. (2023) have shown that using retrieval algorithm GGG2020 instead of GGG2014 reduces XCO_2 bias from 1.3 ppm to 0.5 ppm, which may further explain the discrepancy.

Figure 3 shows the time series of XCH_4 and XCO_2 biases for the ±30° × ±10° box. No systematic changes in biases are observed for most products, except for GOSAT NIES XCO_2, values which exhibited positive biases during December to February and negative biases during April to May. Overall, the biases at the Gadanki are consistent with those reported by O' Dell et al. (2018) for OCO-2 version 8 over TCCON sites (~ 1 ppm).

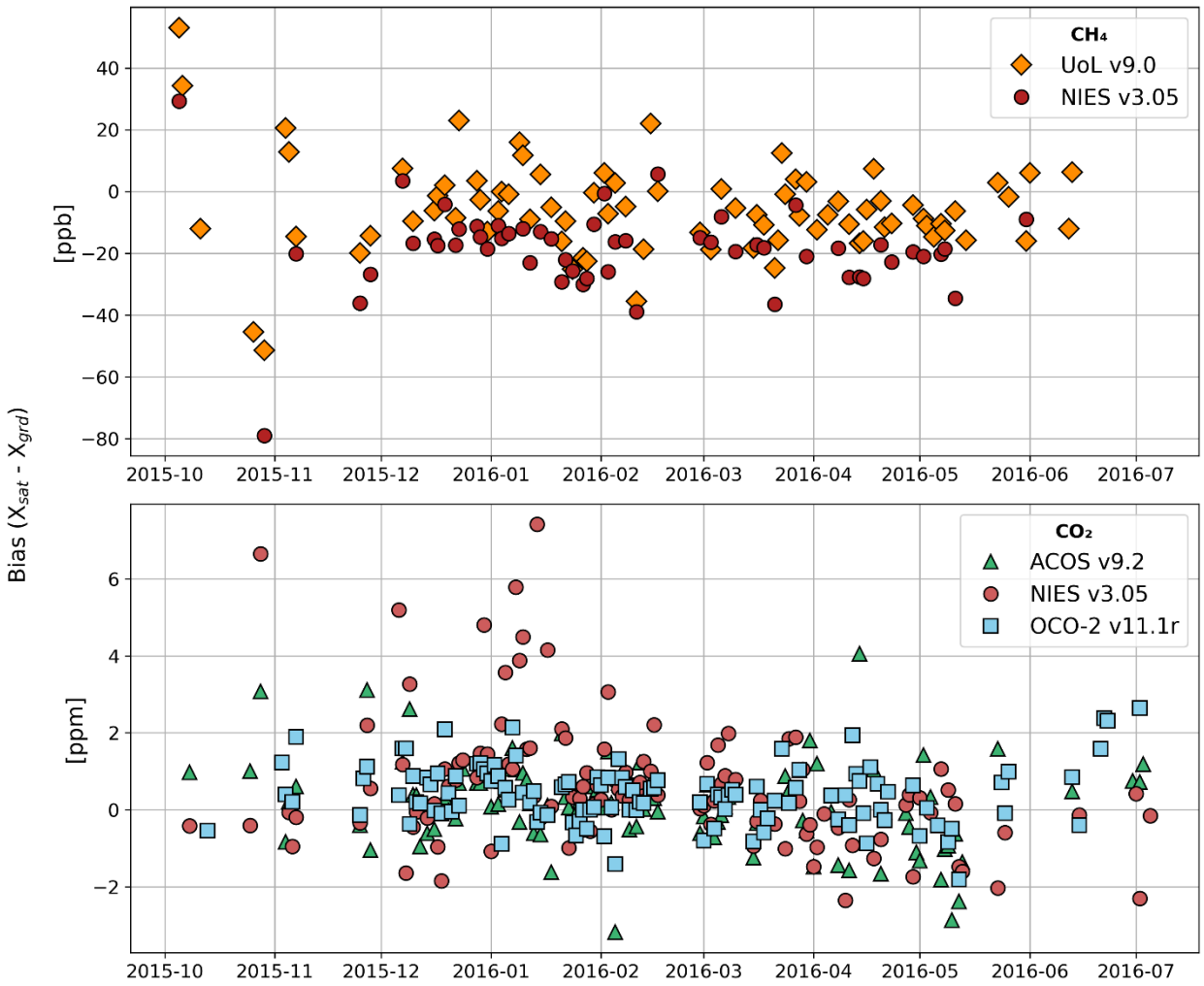

Figure 3: Time series of biases in GOSAT and OCO-2 retrieved XCH_4 (top panel) and XCO_2 (bottom panel) over Gadanki, India. Results are shown for satellite data selected within a ±30° longitude x ±10° latitude region centred on the station.

4.2 Case Studies and Seasonal variations of methane

Figure 4 shows methane mixing ratio enhancements calculated using the FLEXPART model and the ECLIPSEv6+Wet-land inventory. As previously mentioned, the model is configured such that the values represent daytime mean mixing-ratios in the altitude range of 0 to 15 km over Gadanki, contributed by emissions from the preceding 10 days. The altitude range of 0 to 15 km is selected because the tropopause altitude in the tropics is typically between 15 and 18 km (Pandit et al., 2014), and emissions from the past 10 days are generally confined within this range.

The 10-day back trajectory is chosen based on earlier work by Gadhavi et al. (2015), which demonstrated that, for the Gadanki location, a10-day back trajectory captures emissions from almost the entire South Asia. The averaging period is selected as daytime (9 am to 6 pm local time) to ensure a one-to-one correspondence with observed mixing ratios, which are measured using solar radiation through FTS and are therefore only available during daylight hours.

Hereafter, these values will be referred to as model values, However, it is important to note that the model values do not account for the columnar CH_4 mixing ratio resulting from emissions prior to the 10-day period and, therefore, do not represent the total columnar mixing ratio as seen in FTS or satellite data.

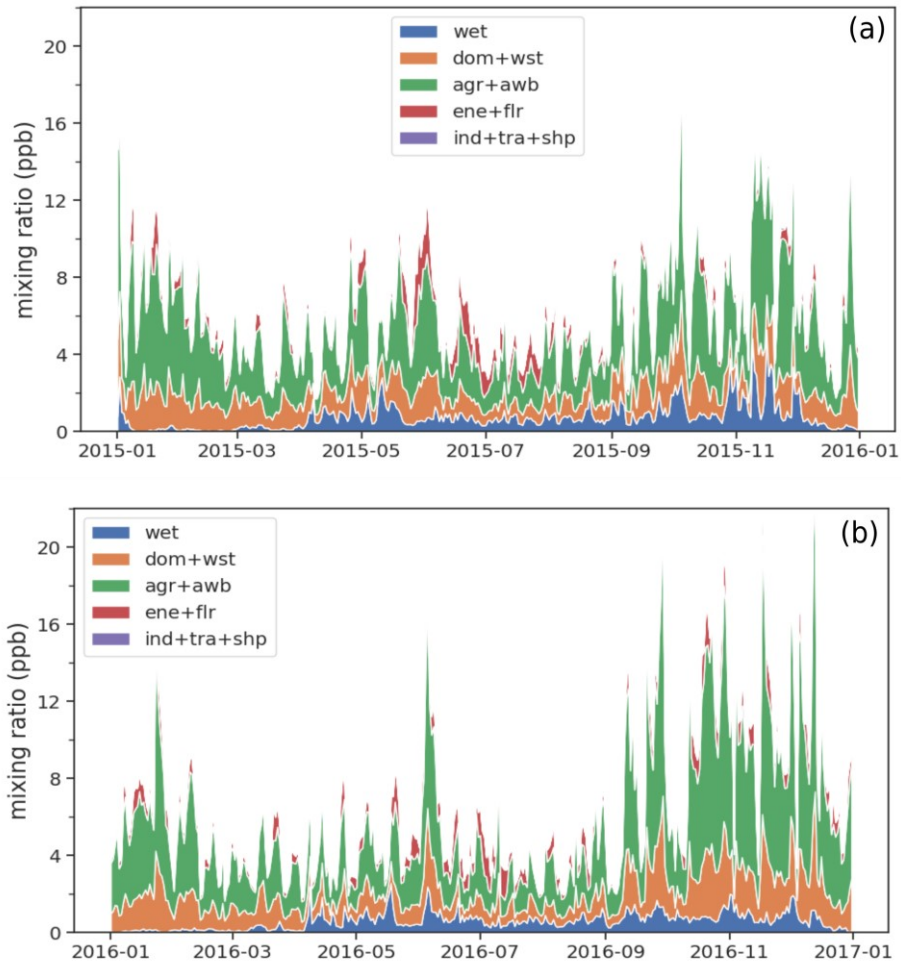

Figure 4: Model calculated columnar (0 to 15km) average methane mixing ratio enhancements due to emissions of past 10 days for year (a) 2015 and (b) 2016. Colours show contribution of different sectors viz. wetland (wet), domestic+waste (dom+wst), agriculture + agricultural waste burning (agr+awb), energy + flaring (ene+flr), and industry + transport + shipping (ind+tra+shp).

Overall, the model estimates methane mixing ratio enhancements ranging from 2 ppb to 26 ppb during 2015 and 2016. While there is significant day-to-day variability, a seasonal pattern is still discernible in the model-calculated values. Typically, the mixing ratio enhancements are high in November, decreases slightly in December, and rise again during January and February. They decrease in March and April, briefly rise in the second half of May, and then decrease again, remaining low from June to September. The mixing ratios rise again in October, peaking in November. Sector-wise, wetlands do not show large seasonal variations. Wetland contributions are low from December to March. In other seasons, wetland contributions occasionally reach as high as 40% of total mixing ratios, but for most part of the year, they remain around 10%. The highest contribution comes from the agriculture sector, accounting for nearly 55% of the total mixing ratio enhancements, followed by the waste sector, which contributes about 17% to the model values at Gadanki. The domestic and energy sectors contribute about 5% each. The domestic sector's contribution is lower in July and August, mainly due to the air masses originating from the west of Gadanki in peninsular India, where the population is smaller and contributes less to methane emissions. Flaring contributes negligibly for most part of the year, but during June to July, its contribution can reach up to 40%, primarily due to low emissions from other sectors during this period and the winds from the Arabian Sea bringing emissions from oil rigs off the west coast of India, the eastern Arabian Peninsula, and northeastern Africa. Industry, transport, shipping and agricultural waste burning activities contribute less than 1% of atmospheric load of methane at Gadanki.

Figure 5 shows model-calculated methane mixing ratio (ΔXCH_4; solid blue line; left Y-axis) and the methane mixing ratios (XCH_4) observed using FTS (red filled circles; right Y-axis) in a single plot. The left Y-axis represents the model mixing ratio, which only accounts for emissions from the preceding 10 days. For lack of a better term, we refer to it as ΔXCH_4. The right Y-axis shows the observed values in ppm. As mentioned earlier, the model was configured to reflect incremental variability caused by regional emissions. If the background CH_4 mixing ratios were constant, the day-to-day variability relative to background values should be the same in both the model and the observations. However, we observe differences in both the absolute values of variability and their seasonal patterns. Several sudden increases in the model values, which appear as spikes in **Figure** 5 (e.g. 5 October 2015 and 27 December 2015), correspond to variations in the observations. While the observations are not as continuous as model values and cannot capture all the variability seen in the model, some degree of day-to-day variability is correlated between the model and observations ($R^2 = 0.35$). However, the magnitude of variability between the model and observed values is quite different. For instance, the observed mixing ratios from 5 October 2015 to 8 October 2015 decreased by 49 ppb, whereas the model values during the same period decreased only by 16 ppb. Over the entire observation period, total column methane mixing ratios varied by 100 ppb, while the model values which excludes background mixing ratios varied only by 20 ppb. This discrepancy may be due to two main factors: either the emission fluxes in the emission inventory are underestimated, or the background mixing ratios are not constant. The latter factor could explain the mismatch on a monthly scale. Starting in October 2015, both model and observed values are high and decrease toward June-July 2016. While the model values are already low by March 2016, the observed values decrease gradually from November 2015 to January 2016, remain nearly constant from January 2016 to April 2016, and then decrease rapidly in May, reaching a minimum during the last week of June and the first week of July.

Chandra et al. (2017) analysed methane variations over different parts of India using Japan Agency for Marine-earth Science and TEChnology (JAMSTEC)'s Atmospheric Chemical Transport Model. They found that, over South India, although 60% of the columnar concentration is attributed to CH_4 in the lower troposphere, there is very little correlation between regional emissions and columnar methane variations. This was attributed to changes in atmospheric chemistry and transport. According to Chandra et al. (2017), the methane loss rate increases from 6 ppb day^{-1} in January to 12 ppb day^{-1} from April to September. Additionally, anticyclonic winds in the upper troposphere confine uplifted methane molecules over broader South Asia during the monsoon season, contributing significantly to methane over Western India, but not significantly over South India. Since FLEXPART doesn't include chemistry other than the reaction with OH radical, lower decrease in model values from March to July could be due to absence of chemistry as well as transport of background methane.

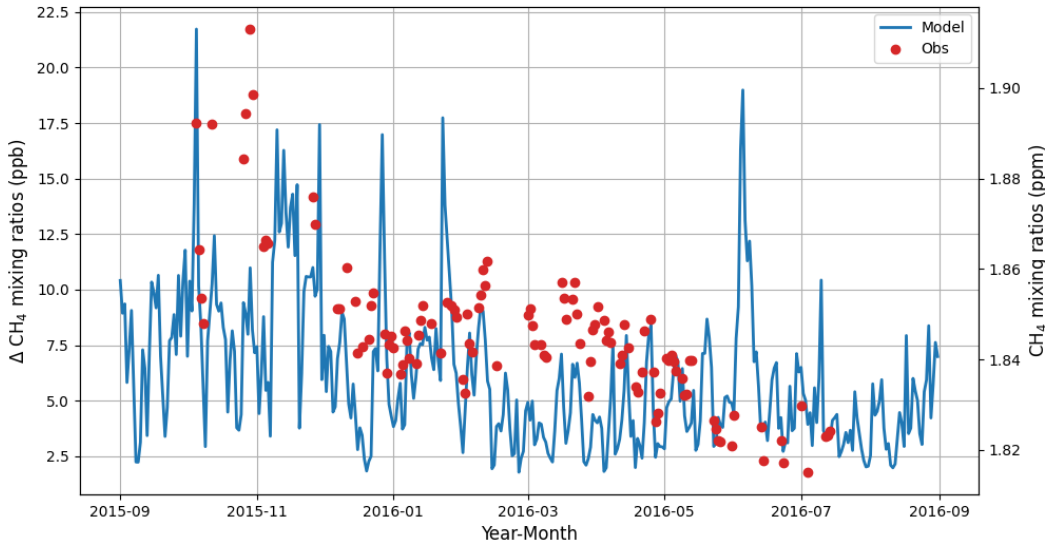

Figure 5: Observed and modelled mixing ratios at Gadanki. (The left-hand y-axis shows value for modelled mixing ratio and right-hand axis shows value for observed mixing ratios

5 Conclusions and Outlook

The GOSAT and OCO-2 satellites provide global coverage of columnar mixing ratios of CO_2 and CH_4 every 3 and 15 days, respectively. These data are crucial for deriving regional greenhouse gas emission fluxes. However, the accuracy of the derived emission fluxes strongly depends on the precision and accuracy of the satellite products. In our study, we compared GOSAT and OCO-2 satellite-measured columnar mixing ratios of CO_2 and CH_4 with ground-based FTS measurements from a location in South India.

The biases in methane mixing ratios estimated using the GOSAT satellite ranged from -0.6 ppb to -18.5 ppb, depending on the product and matching criteria used for the collocation of ground and satellite footprints. Even though NIES and UoL XCH_4 dry-air mole fraction derived from same satellite (GOSAT), UoL XCH_4 data has much smaller biases for corresponding spatial box-sizes. The biases in UoL XCH_4 meet ESA's CCI requirement for systematic errors (< 10 ppb) for all the matching criteria, NIES XCH_4 meet the requirement only for intermediate longitude-latitude box size.

Again, NIES XCO_2 and ACOS XCO_2 products are derived from same satellite (GOSAT), NIES XCO_2 product does not meet the CCI's systematic error requirement of <0.5 ppm, whereas ACOS XCO_2 data product not only met the CCI's systematic error requirement, it had the lowest biases among the three XCO_2 datasets evaluated. Both the ACOS and OCO-2 data meet ESA's CCI requirement for CO_2 biases (< 0.5 ppm), while the NIES XCO_2 v3.05 values showed higher biases, ranging from 0.644 ppm to 0.983 ppm. The precision requirement of < 8 ppm for XCO_2 set by ESA CCI was met by all three datasets with a significant margin, with scatter values ranging from 0.776 ppm to 1.88 ppm.

We used to model to understand seasonal changes resulting from local and regional emissions in methane mixing ratios and sectoral composition of the sources. The model captures the overall seasonal variation in methane enhancements—showing peaks during certain months (e.g., November) and lows during others (e.g., June–July). Agriculture sector is contributing about 55% on average, followed by sectors such as waste and wetlands.

When comparing the model estimated season variability (ΔXCH_4, which represent only the contribution from emissions in the preceding 10 days) with the observed seasonal changes in the total columnar mixing ratios, the model tends to exhibit a much narrower range of variability. For example, over a given period, the observations show a change of about 100 ppb, while the model shows only around a 20 ppb change. This discrepancy suggests that there are significant changes

in background methane mixing ratios with season which might limit use of inverse modelling techniques to estimate emission fluxes.

Overall, our study demonstrates that satellite-based greenhouse gas estimates over South Asia show promising accuracy and precision for emission flux retrievals. In recent years, several new satellites from both public and private organizations have been launched to provide greenhouse gas estimates. This highlights the need for sustained efforts to establish a wider and denser network of Fourier Transform Spectrometer (FTS) across South Asia, which can be used for satellite and model validations with implication for better assessment of GHGs emissions and improved climate modelling.

Code availability

PROFFAST Code used to retrieve columnar concentration of GHGs from raw interferograms is publicly available. The link is provided in the main text as well as in acknowledgement section. Source code of FLEXPART model is publicly available. The link for FLEXPART is provided in the main text and in the acknowledgement section.

Data availability

Satellite data are publicly available and their links are provided in main text as well as in acknowledgement. Data of ground-based Fourier transform spectrometer will be made available through institute's website or through public repository soon. Currently, they can be obtained by writing email to HG.

Author contribution

HG, AJ, and FH conceptualised the study. HG, CJ, MS and MF did data curation. HG carried out formal analysis. HG and AA carried out model runs and analysis of model output. HG prepared visualization and wrote original draft. SR, CJ, AJ and FH reviewed and edited the draft.

Competing interests

One of the authors is a member of the editorial board of journal Atmospheric Measurement and Techniques.

Acknowledgements

Authors gratefully acknowledges following dataset and software providers and their funding agencies. Physical Research Laboratory is supported by the Department of Space, Government of India. The ERA-Interim reanalysis dataset, Copernicus Climate Change Service (C3S) available from https://www.ecmwf.int/en/forecasts/dataset/ecmwf-reanalysis-interim were used to run FLEXPART model (ECMWF, 2011), A priori profiles of pressure, temperature and species were obtained from CalTechFtp Server (https://tccon-wiki.caltech.edu/Main/ObtainingGinputData). GOSAT satellite data were obtained from NIES website http://www.gosat.nies.go.jp/. OCO-2 satellite data used in this study were produced by the OCO-2 project at the Jet Propulsion Laboratory, California Institute of Technology, and obtained from the OCO-2 data archive maintained at the NASA Goddard Earth Science Data and Information Services Center (OCO-2 Science Team, 2019). Source code of FLEXPART model was obtained from https://www.flexpart.eu. ECLIPSEv6b inventory data were provided by International Institute of Applied System Analysis through its website (https://iiasa.ac.at/models-

tools-data/global-emission-fields-of-air-pollutants-and-ghgs). WetCHARTs version 1.0 – wetlands emission inventory data were provided by Oak Ridge National Laboratory's Distributed Active Archive Center (ORNL DAAC) through their web-site (https://daac.ornl.gov/). The PROFFAST v2.4 and PROFFASTpylot software are open source software developed at KIT under framework of ESA's COCCON-PROCEEDS project. These software are available at https://www.imk-asf.kit.edu/english/3225.php and https://gitlab.eudat.eu/coccon-kit/proffastpylot. Authors thank Darko Dubravica and Benedikt Herkommer for help with PROFFAST algorithm.

References

Abrams, M. C., Toon, G. C., & Schindler, R. A. (1994). Practical example of the correction of Fourier-transform spectra for detector nonlinearity. *Appl. Opt.*, 33, 6307–6314. https://doi.org/10.1364/AO.33.006307.

Alberti, C., Hase, F., Frey, M., Dubravica, D., Blumenstock, T., Dehn, A., et al. (2022a). Improved calibration procedures for the EM27/SUN spectrometers of the COllaborative Carbon Column Observing Network (COCCON). *Atmos. Meas. Tech.*, 15, 2433–2451. https://doi.org/10.5194/amt-15-2433-2022.

Alberti, C., Tu, Q., Hase, F., Makarova, M. V., Gribanov, K., Foka, S. C., Zakharov, V., Blumenstock, T., Buchwitz, et al. (2022b), Investigation of spaceborne trace gas products over St Petersburg and Yekaterinburg, Russia, by using COllaborative Column Carbon Observing Network (COCCON) observations, *Atmos. Meas. Tech.*, 15, 2199–2229, https://doi.org/10.5194/amt-15-2199-2022.

Amann, M., Bertok, I., Borken-Kleefeld, J., Cofala, J., Heyes, C., Höglund-Isaksson, L., et al. (2011). Cost-effective control of air quality and greenhouse gases in Europe: Modeling and policy applications. *Environmental Modelling & Software*, 26, 1489–1501. https://doi.org/10.1016/j.envsoft.2011.07.012

Amann, M., J. Borken-Kleefeld, J. Cofala, C. Heyes, Z. Klimont, P. Rafaj, P. Purohit, W. Schöpp, and W. Winiwarter (2012), Future emissions of air pollutants in Europe – Current legislation baseline and the scope for further reductions, TSAP Report #1, International Institute for Applied Systems Analysis, Laxenburg, Austria.

Bergamaschi, P., C. Frankenberg, J. Meirink, M. Krol, F. Dentener, T. Wagner, U. Platt, J. Kaplan, S. Körner, M. Heimann, et al. (2007), Satellite chartography of atmospheric methane from SCIAMACHY on board ENVISAT: 2. Evaluation based on inverse model simulations, *J. Geophys. Res. Atmos.*, 112, https://doi.org/10.1029/2006JD007268.

Bergamaschi, P., C. Frankenberg, J. F. Meirink, M. Krol, M. G. Villani, S. Houweling, F. Dentener, E. J. Dlugokencky, J. B. Miller, L. V. Gatti, A. Engel, and I. Levin (2009), Inverse modeling of

global and regional CH4 emissions using SCIAMACHY satellite retrievals, *J. Geophys. Res.*, 114, https://doi.org/10.1029/2009JD012287.

Bloom, A. A., Exbrayat, J.-F., van der Velde, I. R., Feng, L., & Williams, M. (2016). The decadal state of the terrestrial carbon cycle: Global retrievals of terrestrial carbon allocation, pools, and residence times. *Proc. Natl. Acad. Sci. U.S.A.*, 113, 1285–1290. https://doi.org/10.1073/pnas.1515160113.

Bloom, A. A., K. W. Bowman, M. Lee, A. J. Turner, R. Schroeder, J. R. Worden, R. Weidner, K. C. McDonald, and D. J. Jacob (2017a), A global wetland methane emissions and uncertainty dataset for atmospheric chemical transport models (WetCHARTs version 1.0), *Geosci. Model Dev.*, 10, 2141–2156, https://doi.org/10.5194/gmd-10-2141-2017.

Bloom, A. A., K. Bowman, M. Lee, A. J. Turner, R. Schroeder, J. R. Worden, R. J. Weidner, K. C. McDonald, and D. J. Jacob (2017b), CMS: Global 0.5-deg Wetland Methane Emissions and Uncertainty (WetCHARTs v1.0), *ORNL DAAC*, Oak Ridge, Tennessee, USA, https://doi.org/10.3334/ORNLDAAC/1502.

Bousquet, P., B. Ringeval, I. Pison, E. Dlugokencky, E. Brunke, C. Carouge, F. Chevallier, A. Fortems-Cheiney, C. Frankenberg, D. Hauglustaine, et al. (2010), Source attribution of the changes in atmospheric methane for 2006–2008, *Atmos. Chem. Phys.*, 10, 27603–27630, https://doi.org/10.5194/acp-10-27603-2010.

Buchwitz, M., B. Dils, H. Boesch, D. Brunner, A. Butz, C. Crevoisier, R. Detmers, C. Frankenberg, O. Hasekamp, W. Hewson, A. Laeng, S. Noël, J. Notholt, R. Parker, M. Reuter, O. Schneising, P. Somkuti, A.-M. Sundström, and E. D. Wachter (2017), Product validation and intercomparison report for essential climate variable greenhouse gases for data set climate research data package no. 4, *ESA Climate Change Initiative*, [Online] Available: http://www.esa-ghg-cci.org/?q=webfm_send/352. (last accessed on 1 Feb 2024).

Chandra, N., S. Hayashida, T. Saeki, and P. K. Patra (2017), What controls the seasonal cycle of columnar methane observed by GOSAT over different regions in India?, *Atmos. Chem. Phys.*, 17, 12633–12643, https://doi.org/10.5194/acp-17-12633-2017.

Chevallier, F., P. Bergamaschi, S. Houweling, T. van Leeuwen, and P. I. Palmer (2016), User requirements document for the GHG-CCI project of ESA's Climate Change Initiative, *GHG-CCI*, [Online] Available: http://www.esa-ghg-cci.org.

549 Chevallier, F., M. Fisher, P. Peylin, S. Serrar, P. Bousquet, F.-M. Bréon, A. Chédin, and P. Ciais
550 (2005), Inferring CO2 sources and sinks from satellite observations: Method and application to
551 TOVS data, *J. Geophys. Res. Atmos.*, 110, https://doi.org/10.1029/2005JD006390.

552 Crisp, D., R. M. Atlas, F.-M. Breon, L. R. Brown, J. P. Burrows, P. Ciais, B. J. Connor, S. C. Doney,
553 I. Y. Fung, D. J. Jacob, C. E. Miller, D. O'Brien, S. Pawson, J. T. Randerson, P. Rayner, R. J.
554 Salawitch, S. P. Sander, B. Sen, G. L. Stephens, P. P. Tans, G. C. Toon, P. O. Wennberg, S. C. Wofsy,
555 Y. L. Yung, Z. Kuang, B. Chudasama, G. Sprague, B. Weiss, R. Pollock, D. Kenyon, S. Schroll
556 (2004), The Orbiting Carbon Observatory (OCO) mission, *Adv. Space Res.*, 34, 700–709,
557 https://doi.org/10.1016/j.asr.2003.08.062.

558 Crisp, D., H. R. Pollock, R. Rosenberg, L. Chapsky, R. A. M. Lee, F. A. Oyafuso, C. Frankenberg,
559 C. W. O'Dell, C. J. Bruegge, G. B. Doran, A. Eldering, B. M. Fisher, D. Fu, M. R. Gunson, L.
560 Mandrake, G. B. Osterman, F. M. Schwandner, K. Sun, T. E. Taylor, P. O. Wennberg, and D. Wunch
561 (2017), The on-orbit performance of the Orbiting Carbon Observatory-2 (OCO-2) instrument and
562 its radiometrically calibrated products, *Atmos. Meas. Tech.*, 10, 59–81, https://doi.org/10.5194/amt-
563 10-59-2017.

564 Crisp, D., C. O'Dell, A. Eldering, B. Fisher, F. Oyafuso, V. Payne, et al. (2021), Orbiting carbon
565 observatory (OCO) - 2 Level 2 Full Physics Algorithm Theoretical Basis Document, *Jet Propulsion*
566 *Laboratory, California Institute of Technology* under contract with NASA, Pasadena, California.

567 Dee, D. P., S. M. Uppala, A. J. Simmons, P. Berrisford, P. Poli, S. Kobayashi, et al. (2011), The
568 ERA-Interim reanalysis: configuration and performance of the data assimilation system, *Q. J. R.*
569 *Meteorol. Soc.*, 137(656), 553–597, https://doi.org/10.1002/qj.828.

570 Dietrich, F., Chen, J., Voggenreiter, B., Aigner, P., Nachtigall, N., and Reger, B.: MUCCnet (2021),
571 Munich Urban Carbon Column network, *Atmos. Meas. Tech.*, 14, 1111–1126,
572 https://doi.org/10.5194/amt-14-1111-2021.

573 Dunn, R., F. Aldred, N. Gobron, et al. (2022), Global Climate, *Bull. Am. Meteorol. Soc.*, 103(8),
574 S11–S142, https://doi.org/10.1175/bams-d-22-0092.1.

575 European Centre for Medium-range Weather Forecast (ECMWF, 2011): The ERA-Interim
576 reanalysis dataset, Copernicus Climate Change Service (C3S) (accessed 30 July 2019), available
577 from https://www.ecmwf.int/en/forecasts/dataset/ecmwf-reanalysis-interim.

578 Feld, L., Herkommer, B., Vestner, J., Dubravica, D., Alberti, C., & Hase, F. (2024),
579 PROFFASTpylot: Running PROFFAST with Python. *Journal of Open Source Software*, 9, 6481,
580 https://doi.org/10.21105/joss.06481.

Fiore, A. M., D. J. Jacob, B. D. Field, D. G. Streets, and S. D. Fernandes (2002), Linking ozone pollution and climate change: The case for controlling methane, *Geophys. Res. Lett.*, 29, 1919, https://doi.org/10.1029/2002GL015601.

Fleming, E. L., C. George, D. E. Heard, C. H. Jackman, M. J. Kurylo, W. Mellouki, et al. (2015), The impact of current CH4 and N2O atmospheric loss process uncertainties on calculated ozone abundances and trends, *J. Geophys. Res. Atmos.*, 120, 5267 – 5293, https://doi.org/10.1002/2014JD022067.

Frausto-Vicencio, I., Heerah, S., Meyer, A. G., Parker, H. A., Dubey, M., and Hopkins, F. M. (2023), Ground solar absorption observations of total column CO, CO2, CH4, and aerosol optical depth from California's Sequoia Lightning Complex Fire: emission factors and modified combustion efficiency at regional scales, *Atmos. Chem. Phys.*, 23, 4521–4543, https://doi.org/10.5194/acp-23-4521-2023.

Frey, M., M. K. Sha, F. Hase, M. Kiel, T. Blumenstock, R. Harig, G. Surawicz, N. M. Deutscher, K. Shiomi, J. E. Franklin, H. Bösch, J. Chen, M. Grutter, H. Ohyama, Y. Sun, A. Butz, G. Mengistu Tsidu, D. Ene, D. Wunch, Z. Cao, O. Garcia, M. Ramonet, F. Vogel, and J. Orphal (2019), Building the COllaborative Carbon Column Observing Network (COCCON): long-term stability and ensemble performance of the EM27/SUN Fourier transform spectrometer, *Atmos. Meas. Tech.*, 12, 1513–1530, https://doi.org/10.5194/amt-12-1513-2019.

Gadhavi, H. S., Renuka, K., Kiran, V. R., Jayaraman, A., Stohl, A., Klimont, Z., & Beig, G. (2015). Evaluation of black carbon emission inventories using a Lagrangian dispersion model –“ a case study over southern India. *Atmos. Chem. Phys.*, 15, 1447–1461. https://doi.org/10.5194/acp-15-1447-2015.

GCOS-200 (2016): The global observing system for climate: Implementation needs, *World Meteorological Organization*.

Gisi, M., F. Hase, S. Dohe, and T. Blumenstock (2011), Camtracker: a new camera controlled high precision solar tracker system for FTIR-spectrometers, *Atmos. Meas. Tech.*, 4, 47–54, https://doi.org/10.5194/amt-4-47-2011.

Gisi, M., F. Hase, S. Dohe, T. Blumenstock, A. Simon, and A. Keens (2012), XCO_2 measurements with a tabletop FTS using solar absorption spectroscopy, *Atmos. Meas. Tech.*, 5, 2969–2980, https://doi.org/10.5194/amt-5-2969-2012.

Hase, F., T. Blumenstock, and C. Paton-Walsh (1999), Analysis of the instrumental line shape of high-resolution Fourier transform IR spectrometers with gas cell measurements and new retrieval software, *Appl. Opt.*, 38, 3417 – 3422, https://doi.org/10.1364/AO.38.003417.

Hase, F., J. W. Hannigan, M. T. Coffey, A. Goldman, M. Höpfner, N. B. Jones, C. P. Rinsland, and S. W. Wood (2004), Intercomparison of retrieval codes used for the analysis of high-resolution, ground-based FTIR measurements, *J. Quant. Spectrosc. Radiat. Transf.*, 87, 25–52, https://doi.org/10.1016/j.jqsrt.2003.12.008.

Herkommer, B., Alberti, C., Castracane, P., Chen, J., Dehn, A., Dietrich, F., Deutscher, N. M., Frey, M. M., et al. (2024), Using a portable FTIR spectrometer to evaluate the consistency of Total Carbon Column Observing Network (TCCON) measurements on a global scale: the Collaborative Carbon Column Observing Network (COCCON) travel standard, *Atmos. Meas. Tech.*, 17, 3467–3494, https://doi.org/10.5194/amt-17-3467-2024.

Hoglund-Isaksson, L. (2012), Global anthropogenic methane emissions 2005–2030: technical mitigation potentials and costs, *Atmos. Chem. Phys.*, 12, 9079–9096, https://doi.org/10.5194/acp-12-9079-2012.

IPCC 2008, 2006 IPCC Guidelines for National Greenhouse Gas Inventories – A primer, Prepared by the National Greenhouse Gas Inventories Programme, Eggleston H.S., Miwa K., Srivastava N. and Tanabe K. (eds)., IGES, Japan., 20 pp., ISBN 9784887880320.

IMK-ASF, K. (2024a, February 28). Data Processing. Retrieved from https://www.imk-asf.kit.edu/english/3225.php.

IMK-ASF, K. (2024b). PROFFASTpylot v1.3 documentation. Retrieved from https://www.imk-asf.kit.edu/english/4261.php.

Jacobs, N., O'Dell, C. W., Taylor, T. E., Logan, T. L., Byrne, B., Kiel, M., et al. (2024). The importance of digital elevation model accuracy in XCO_2 retrievals: improving the Orbiting Carbon Observatory 2 Atmospheric Carbon Observations from Space version 11 retrieval product. *Atmospheric Measurement Techniques*, *17*(5), 1375–1401. https://doi.org/10.5194/amt-17-1375-2024.

Jain, C. D., V. Singh, S. T. Akhil Raj, B. L. Madhavan, and M. V. Ratnam (2021), Local emission and long-range transport impacts on the CO, CO2, and CH4 concentrations at a tropical rural site, *Atmos. Environ.*, 254, 118397, https://doi.org/10.1016/j.atmosenv.2021.118397.

641 Jayaraman, A., M. V. Ratnam, A. K. Patra, T. N. Rao, S. Sridharan, M. Rajeevan, et al. (2010),
642 Study of Atmospheric Forcing and Responses (SAFAR) campaign: overview, *Annales Geophysicae*,
643 28, 89–101, https://doi.org/10.5194/angeo-28-89-2010.

644 Kavitha, M., and P. R. Nair (2016), Region-dependent seasonal pattern of methane over Indian
645 region as observed by SCIAMACHY, *Atmos. Environ.*, 131, 316–325,
646 https://doi.org/10.1016/j.atmosenv.2016.02.008.

647 Keppel-Aleks, G., G. C. Toon, P. O. Wennberg, and N. M. Deutscher (2007), Reducing the impact
648 of source brightness fluctuations on spectra obtained by Fourier-transform spectrometry, *Appl. Opt.*,
649 46, 4774–4779, https://doi.org/10.1364/AO.46.004774.

650 Klimont, Z., K. Kupiainen, C. Heyes, P. Purohit, J. Cofala, P. Rafaj, J. Borken-Kleefeld, and W.
651 Schöpp (2017), Global anthropogenic emissions of particulate matter including black carbon,
652 *Atmos. Chem. Phys.*, 17, 8681–8723, https://doi.org/10.5194/acp-17-8681-2017.

653 Laughner, J. L., J. L. Neu, D. Schimel, P. O. Wennberg, K. Barsanti, K. W. Bowman, et al. (2021),
654 Societal shifts due to COVID-19 reveal large-scale complexities and feedbacks between
655 atmospheric chemistry and climate change, *Proc. Natl. Acad. Sci. U.S.A.*, 118,
656 https://doi.org/10.1073/pnas.2109481118.

657 Laughner, J. L., G. C. Toon, J. Mendonca, C. Petri, S. Roche, D. Wunch, et al. (2024). The Total
658 Carbon Column Observing Network's GGG2020 data version. Earth System Science Data, 16(5),
659 2197–2260. https://doi.org/10.5194/essd-16-2197-2024

660 Messerschmidt, J., R. Macatangay, J. Notholt, C. Petri, T. Warneke, and C. Weinzierl (2010), Side
661 by side measurements of CO2 by ground-based Fourier transform spectrometry (FTS), *Tellus B:*
662 *Chem. Phys. Meteorol.*, 62, 749–758, https://doi.org/10.1111/j.1600-0889.2010.00491.x.

663 Marsh, D., M. Mills, D. E. Kinnison, and J.-F. Lamarque (2013), Climate change from 1850 to 2005
664 simulated in CESM1(WACCM), *J. Climate*, 26, 7372–7391, https://doi.org/10.1175/JCLI-D-12-
665 00558.1.

666 NCEP (2000), National Centers for Environmental Prediction/National Weather
667 Service/NOAA/U.S. Department of Commerce., NCEP FNL Operational Model Global
668 Tropospheric Analyses, continuing from July 1999. Research Data Archive at the National Center
669 for Atmospheric Research, Computational and Information Systems Laboratory. 2000 (updated
670 daily) https://doi.org/10.5065/D6M043C6. Accessed on 15 Sep 2017.

671 Noël, S., K. Weigel, K. Bramstedt, A. Rozanov, M. Weber, H. Bovensmann, and J. P. Burrows
672 (2018), Water vapour and methane coupling in the stratosphere observed using SCIAMACHY solar

673 occultation measurements, *Atmos. Chem. Phys.*, 18, 4463–4476, https://doi.org/10.5194/acp-18-
674 4463-2018.

675 OCO-2 Science Team (2019), OCO-2 Science Team/Michael Gunson, Annmarie Eldering, ACOS
676 GOSAT/TANSO-FTS Level 2 Full Physics Standard Product V9r, Greenbelt, MD, USA, Goddard
677 Earth Sciences Data and Information Services Center (GES DISC), Accessed on 1 January 2024,
678 10.5067/OSGTIL9OV0PN.

679 O'Dell, C. W., A. Eldering, P. O. Wennberg, D. Crisp, M. R. Gunson, B. Fisher, et al. (2018),
680 Improved retrievals of carbon dioxide from Orbiting Carbon Observatory-2 with the version 8
681 ACOS algorithm, *Atmos. Meas. Tech.*, 11, 6539–6576, https://doi.org/10.5194/amt-11-6539-2018.

682 Olsen, K. S., K. Strong, K. A. Walker, C. D. Boone, P. Raspollini, J. Plieninger, et al. (2017),
683 Comparison of the GOSAT TANSO-FTS TIR CH_4 volume mixing ratio vertical profiles with those
684 measured by ACE-FTS, ESA MIPAS, IMK-IAA MIPAS, and 16 NDACC stations, *Atmos. Meas.*
685 *Tech.*, 10, 3697–3718, https://doi.org/10.5194/amt-10-3697-2017.

686 Osterman, G., A. Eldering, C. Cheng, C. O'Dell, D. Crisp, C. Frankenberg, and B. Fisher (2017),
687 ACOS Level 2 standard product and Lite data product data user's guide, v7.3, 51 pp.

688 Pak, N. M., Hedelius, J. K., Roche, S., Cunningham, L., Baier, B., Sweeney, C., Roehl, C.,
689 Laughner, et al. (2023), Using portable low-resolution spectrometers to evaluate Total Carbon
690 Column Observing Network (TCCON) biases in North America, *Atmos. Meas. Tech.*, 16, 1239–
691 1261, https://doi.org/10.5194/amt-16-1239-2023.

692 Pandit, A. K., Gadhavi, H., Ratnam, M. V., Jayaraman, A., Raghunath, K., and Rao, S. V. B. (2014).
693 Characteristics of cirrus clouds and tropical tropopause layer: Seasonal variation and long-term
694 trends. *J Atmos and Solar-Terrestrial Phys*, 121, 248–256,
695 https://doi.org/10.1016/j.jastp.2014.07.008

696 Pandit, A. K., H. S. Gadhavi, M. V. Ratnam, K. Raghunath, S. V. B. Rao, and A. Jayaraman (2015),
697 Long-term trend analysis and climatology of tropical cirrus clouds using 16 years of lidar data set
698 over Southern India, *Atmos. Chem. Phys.*, 15, 13833–13848, https://doi.org/10.5194/acp-15-13833-
699 2015.

700 Parker, R. J., A. Webb, H. Boesch, P. Somkuti, R. Barrio Guillo, A. Di Noia, et al. (2020), A decade
701 of GOSAT Proxy satellite CH_4 observations, Earth Syst. Sci. Data, 12, 3383–3412,
702 https://doi.org/10.5194/essd-12-3383-2020.

703 Pathakoti, M., D.V., M., A.L., K., K.S., R., Taori, A., Bothale, R. V., & Chauhan, P. (2024),
704 Temporal variability of atmospheric columnar CO_2, CH_4, CO and N_2O concentrations using ground-

based remote sensing FTIR Spectrometer, *Advances in Space Research*, 73, 4967–4975, https://doi.org/10.1016/j.asr.2024.02.028.

Payne, V., A. Chatterjee, R. Rosenberg, M. Kiel, B. Fisher, L. Dang, et al. (2023), Orbiting carbon observatory-2 & 3 (OCO-2 & OCO-3) Data Product User's Guide, Operational Level 2 Lite Files, *Jet Propulsion Laboratory, California Institute of Technology*, Pasadena, California.

Pisso, I., E. Sollum, H. Grythe, et al. (2019), The Lagrangian particle dispersion model FLEXPART version 10.4, *Geosci. Model Dev.*, 12, 4955–4997, https://doi.org/10.5194/gmd-12-4955-2019.

Renuka, K., H. Gadhavi, A. Jayarman, S. V. B. Lal, M. Naja, and S. V. B. Rao (2014), Study of ozone and NO2 over Gadanki - a rural site in South India, *J. Atmos. Chem.*, 71, 95–112, https://doi.org/10.1007/s10874-014-9284-y.

Renuka, K., H. Gadhavi, A. Jayaraman, S. V. B. Rao, and S. Lal (2020), Study of mixing ratios of SO2 in a tropical rural environment in south India, *J. Earth Syst. Sci.*, 129, https://doi.org/10.1007/s12040-020-1366-4.

Rodgers, C. D. (2000), Inverse Methods for Atmospheric Sounding: Theory and Practice, *Series on Atmospheric, Oceanic and Planetary Physics*, World Scientific Publishing Company.

Sagar, V. K., Pathakoti, M., D.V., M., K.S., R., M.V.R., S. S., Hase, F., et al. (2022), Ground-based remote sensing of total columnar CO_2, CH_4 and CO using EM27/SUN FTIR spectrometer at a suburban location (Shadnagar) in India and validation of Sentinel-5P/TROPOMI, *IEEE Geoscience and Remote Sensing Letters*, 19, 1–5, https://doi.org/10.1109/LGRS.2022.3171216.

Schroeder, R., K. C. McDonald, B. D. Chapman, K. Jensen, E. Podest, Z. D. Tessler, et al. (2015), Development and evaluation of a multi-year fractional surface water data set derived from active/passive microwave remote sensing data, *Remote Sensing*, 7, 16688–16732, https://doi.org/10.3390/rs71215843.

Sepúlveda, E., M. Schneider, F. Hase, O. E. Garcia, A. Gomez-Pelaez, S. Dohe, T. Blumenstock, and J. C. Guerra (2012), Long-term validation of tropospheric column-averaged CH_4 mole fractions obtained by mid-infrared ground-based FTIR spectrometry, Atmos. Meas. Tech., 5, 1425–1441, https://doi.org/10.5194/amt-5-1425-2012.

Sha, M. K., Langerock, B., Blavier, J.-F. L., Blumenstock, T., Borsdorff, T., Buschmann, M., et al. (2021). Validation of methane and carbon monoxide from Sentinel-5 Precursor using TCCON and NDACC-IRWG stations. *Atmos. Meas. Tech.*, *14*(9), 6249–6304. https://doi.org/10.5194/amt-14-6249-2021.

Sha, M., M. de Maziere, J. Notholt, T. Blumenstock, et al. (2020), Intercomparison of low- and high-resolution infrared spectrometers for ground-based solar remote sensing measurements of total column concentrations of CO_2, CH_4 and CO, *Atmos. Meas. Tech.*, 13, 4791–4839, https://doi.org/10.5194/amt-13-4791-2020.

Someya, Y., Yoshida, Y., Ohyama, H., Nomura, S., Kamei, A., Morino, I., et al. (2023). Update on the GOSAT TANSO–FTS SWIR Level 2 retrieval algorithm. *Atmospheric Measurement Techniques*, *16*(6), 1477–1501. https://doi.org/10.5194/amt-16-1477-2023.

Stohl, A., B. Aamaas, M. Amann, et al. (2015), Evaluating the climate and air quality impacts of short-lived pollutants, *Atmos. Chem. Phys.*, 15, 10529–10566, https://doi.org/10.5194/acp-15-10529-2015.

Suman, M. N. S., H. Gadhavi, V. Ravi Kiran, A. Jayaraman, and S. V. B. Rao (2014), Role of coarse and fine mode aerosols in MODIS AOD retrieval: a case study over southern India, *Atmos. Meas. Tech.*, 7, 907–917, https://doi.org/10.5194/amt-7-907-2014.

Turner, A. J., C. Frankenberg, and E. A. Kort (2019), Interpreting contemporary trends in atmospheric methane, *Proc. Natl. Acad. Sci. U.S.A.*, 116, 2805–2813, https://doi.org/10.1073/pnas.1814297116.

Wunch, D., P. O. Wennberg, G. Osterman, B. Fisher, B. Naylor, C. M. Roehl, et al. (2017), Comparisons of the Orbiting Carbon Observatory-2 (OCO-2) XCO2 measurements with TCCON, *Atmos. Meas. Tech.*, 10, 2209–2238, https://doi.org/10.5194/amt-10-2209-2017.

Yokota, T., Yoshida, Y., Eguchi, N., Ota, Y., Tanaka, T., Watanabe, H., and Maksyutov, S. (2009), Global concentrations of CO_2 and CH_4 retrieved from GOSAT: First preliminary results. *Sola*, 5, 160–163, https://doi.org/10.2151/sola.2009-041.